

Atomic geometry and electronic structure of the Si(100) $2\times 3$ -Eu surface phase

M. Kuzmin,\* R. E. Perälä, P. Laukkanen, and I. J. Väyrynen

*Department of Physics, University of Turku, FIN-20014 Turku, Finland*

(Received 15 March 2005; revised manuscript received 31 May 2005; published 25 August 2005)

The structural and electronic properties of the Eu-induced  $2\times 3$  reconstruction on Si(100) have been investigated by scanning tunneling microscopy (STM), scanning tunneling spectroscopy (STS), and high-resolution Si  $2p$  core-level spectroscopy using synchrotron radiation. STM images of this reconstruction are found to be drastically dependent on the bias voltage and tunneling current. STS measurements show that the  $2\times 3$ -Eu surface is semiconducting. Two occupied states at  $-0.9$  and  $-1.75$  V and three unoccupied states at  $+0.35$ ,  $+0.8$ , and  $+1.5$  V are identified in the  $(dI/dV)/(IV)$  spectrum of this surface. The Si  $2p$  core-level spectra taken at various photon energies and emission angles are revealed to include four surface-related components  $S1-S4$  with core-level shifts of  $-0.54$ ,  $-0.24$ ,  $+0.21$ , and  $+0.51$  eV, respectively. The  $S1$ ,  $S2$ , and  $S4$  components are assigned to first-layer Si atoms in the  $2\times 3$ -Eu structure and the  $S3$  component is shown to arise from the second-layer Si atoms. The results are discussed in the context of structural models reported recently for other metal-induced Si(100) $2\times 3$  reconstructions. Finally, an atomic model is proposed for the  $2\times 3$ -Eu phase.

DOI: 10.1103/PhysRevB.72.085343

PACS number(s): 68.35.Bs, 68.55.Jk, 68.37.Ef, 79.60.-i

## I. INTRODUCTION

A great variety of surface reconstructions can be produced by the adsorption of metal submonolayers on silicon, and their structural and electronic properties have been the subject of continuing interest for the last decades. Among these metal-induced structures, however, several common periodicities can be observed in low-energy electron diffraction (LEED) irrespective of adsorbed species. In particular, the  $2\times 3$  periodicity is found to be induced by Ag,<sup>1,2</sup> alkali,<sup>3-8</sup> alkaline-earth (AEM),<sup>9-16</sup> rare-earth (RE),<sup>17-20</sup> and group-III metals<sup>21-24</sup> on Si(100), and several atomic models have been proposed for these surface phases. In earlier studies, the metal atoms were assumed to reside at specific sites on the intact Si(100) $2\times 1$  surface.<sup>3,5,6,9,12</sup> In contrast, more recent studies performed by scanning tunneling microscopy (STM) have revealed the rearrangement of Si atoms in some  $2\times 3$  reconstructions. Saranin *et al.*<sup>8</sup> have reported the top Si-atom density to be  $1/3$  monolayer (ML) in the Na-induced  $2\times 3$  phase, and proposed a model in which the structure of underlying Si resembles that of hydrogen-terminated Si(100) $1\times 3$  (Ref. 25). Based on dual-polarity STM results, Ojima *et al.*<sup>16</sup> have suggested a model of the  $2\times 3$ -Ba phase in which the Si backbone has a similar structure, although the atomic arrangements of the  $2\times 3$ -Ba and  $2\times 3$ -Na reconstructions are not identical. The  $2\times 3$  phases induced by RE metals [Sm,<sup>17</sup> Yb,<sup>18,19</sup> Nd,<sup>18</sup> and Eu (Ref. 20)] have been recently examined by various techniques, however, the atomic structure of the RE/Si(100) $2\times 3$  phases is still the subject of debate, and therefore, these reconstructions cannot be compared with the Si(100) $2\times 3$  surfaces stabilized by the other adsorbates. Thus it is so far unclear whether the M/Si(100) $2\times 3$  phases have a common structure.

In this study, we thoroughly examined the atomic structure and electronic properties of the Eu-induced Si(100) $2\times 3$  surface phase by STM, scanning tunneling spectroscopy (STS), and core-level photoelectron spectroscopy using synchrotron radiation. Europium is a divalent RE metal whose

electronic configuration ( $4f^7 6s^2$ ) is very similar to that of ytterbium ( $4f^{14} 6s^2$ ). These RE metals, however, induce non-equivalent surface structures on Si(100). A mixture of the  $2\times 3$  and  $2\times 4$  periodicities is observed for Yb,<sup>18,19</sup> whereas the  $2\times 3$  and  $c(2\times 6)$  periodicities are found for Eu.<sup>20</sup> In this regard, Eu is similar to Ba that also forms the  $2\times 3$  and  $c(2\times 6)$  reconstructions on Si(100).<sup>15,16</sup> Therefore, the study of the Eu-induced Si(100) $2\times 3$  reconstruction can contribute to the understanding of the common properties of the  $2\times 3$ -REM and  $2\times 3$ -AEM systems. The paper is organized as follows. The experimental details are given in Sec. II. The STM, STS, and core-level photoemission results as well as their interpretation are described in Sec. III. Finally, we propose a structural model of the  $2\times 3$ -Eu phase in Sec. IV.

## II. EXPERIMENT

The experiments were carried out in two separate ultra-high vacuum (UHV) systems. The STM/STS measurements were performed in the UHV system (a base pressure of  $5\times 10^{-11}$  mbar) equipped with Omicron scanning probe microscope, LEED optics, and x-ray photoelectron spectroscopy facilities. The STM images were taken in the constant-current mode. The tunneling spectra were acquired at every raster point of the topography image and averaged over a scanning area. The photoemission measurements were made on beamline 33 at the MAX-lab synchrotron radiation laboratory in Lund, Sweden. The Si  $2p$  spectra were obtained in the photon energy range  $110\leq h\nu\leq 150$  eV utilizing an angle-resolved high-resolution photoelectron spectrometer. The total instrumental resolution was  $\sim 100$  meV, and the angular resolution was  $\sim 2^\circ$ . All measurements were performed at room temperature (RT).

The Si substrates were cut from a mirror-polished P-doped (100) wafer ( $n$ -type,  $\sim 1-2$   $\Omega$  cm). The samples were carefully outgassed at 873 K for several hours and subsequently flashed at 1473 K to remove surface oxide. After flashing, the cleanness and ordering of Si(100) surface were

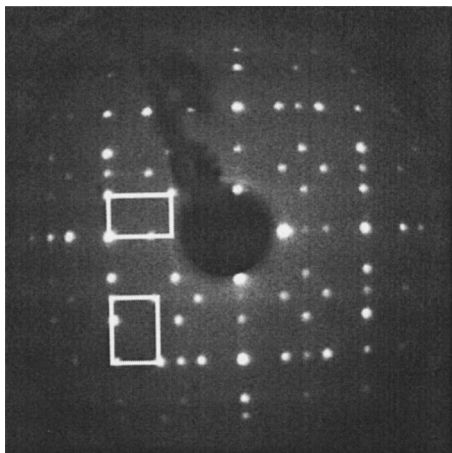


FIG. 1. LEED pattern of  $1/3$ -ML  $\text{Si}(100)2 \times 3$ -Eu surface. Both the  $2 \times 3$  and  $3 \times 2$  domains are shown by line boxes. The electron energy is 52 eV.

verified by LEED, STM, and photoemission. Sample heating was performed by a direct current. The temperature was measured by infrared pyrometers. Europium was deposited from homemade W-coil evaporators. The typical deposition rate was 0.01 ML/s, as measured using a quartz crystal microbalance. One monolayer of Eu was referred to as the density of topmost atoms on the  $\text{Si}(100)2 \times 1$  surface (i.e.,  $1 \text{ ML} = 6.78 \times 10^{14} \text{ atoms/cm}^2$ ). The  $\text{Si}(100)2 \times 3$ -Eu reconstruction was produced by deposition of  $1/3$  ML Eu onto the clean, well-ordered  $\text{Si}(100)2 \times 1$  surface at room temperature, followed by annealing at 873 K. Figure 1 illustrates a typical LEED pattern observed after annealing for 20 min. It shows clear evidence of the double-domain  $2 \times 3$  periodicity (i.e., both  $2 \times 3$  and  $3 \times 2$  domains) with sharp fractional-order spots and a low background intensity. For some samples, LEED showed the  $2 \times 3$  periodicity to coexist with the  $c(2 \times 6)$  one. In particular, the superimposed  $2 \times 3$  and  $c(2 \times 6)$  LEED spots were observed when the sample was heated or/and cooled down with a relatively high temperature ramp. As shown below, both the  $2 \times 3$  and  $c(2 \times 6)$  structures have identical building blocks in a real space and, for this reason, we will refer to the Eu/Si(100) surface with the mixed  $2 \times 3$  and  $c(2 \times 6)$  periodicities as  $2 \times 3$  hereafter.

### III. RESULTS

#### A. STM

Figure 2 represents a typical large-scale ( $35.3 \times 38.7 \text{ nm}^2$ ) filled-state STM image of the  $1/3$ -ML  $\text{Si}(100)2 \times 3$ -Eu surface, taken at a sample bias of  $-1.6 \text{ V}$ . This surface shows up regular rows of protrusions, which are aligned along either the  $[0-11]$  or  $[011]$  direction. The distance between neighboring protrusions in a row is  $2a$  and the distance between adjacent rows is  $3a$ , where  $a = 3.84 \text{ \AA}$  is the unit length of the bulk-terminated  $\text{Si}(100)$  surface. Such a structure is well consistent with the double-domain  $2 \times 3$  periodicity observed in LEED (Fig. 1). Since the STM images taken from the other surface areas revealed the identical

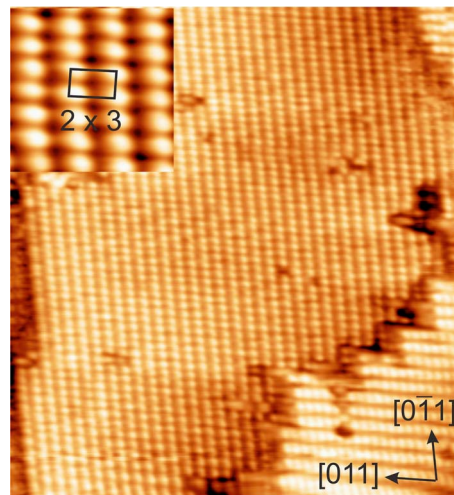


FIG. 2. (Color online) Typical large-scale filled-state STM image ( $35.3 \text{ nm} \times 38.7 \text{ nm}$ ) of  $2 \times 3$ -Eu reconstruction ( $V = -1.6 \text{ V}$ ,  $I = 0.35 \text{ nA}$ ). The inset shows the corrugation of the surface in the filled states with a high magnification ( $3.0 \text{ nm} \times 3.1 \text{ nm}$ ,  $V = -1.4 \text{ V}$ ,  $I = 0.23 \text{ nA}$ ).

structure, we conclude that the Si substrate is entirely covered with the Eu-induced  $2 \times 3$  phase, and that the adsorbate coverage of this phase is  $1/3$  ML. Note that the morphology of this surface, as seen in Fig. 2, is very smooth, which differs from that of the  $\text{Si}(100)2 \times 3$ -Na surface where numerous furrows and islands were observed on terraces.<sup>8</sup>

It is worth noting that in the filled-state STM mode, the  $2 \times 3$ -Eu unit cell includes a single protrusion slightly elongated in the  $\times 3$  direction, as clearly seen in the inset of Fig. 2, and no evidence for additional maxima is found at various negative sample biases. It means that in the filled states, the number of protrusions per  $2 \times 3$  unit does not correspond to that of Eu atoms, because there are two Eu atoms per  $2 \times 3$  mesh at  $1/3$  ML. Recently, it was reported that the electric field induced by the apex of the STM tip can affect the position of adsorbed atoms, and their directional motion driven by the gradient of the electric field in the tip-sample gap was experimentally observed (Ref. 24 and references therein). Taking into account that the Eu atoms gain a positive charge on the Si substrate and the bias voltage applied to the STM tip in the filled-state mode has a positive polarity, the Eu atoms might move outward the region underneath the tip apex, and it can affect the number of STM maxima observed in the filled-state images. We emphasize, however, that the topography of the  $2 \times 3$ -Eu surface observed in the empty-state STM mode was found unchanged after scanning the same area in the filled-state mode, and therefore, it is believed that the filled-state STM images reflect the “true” corrugation of  $2 \times 3$ -Eu surface in occupied orbitals.

A more sophisticated arrangement of the  $2 \times 3$  unit cell is observed in the empty-state images where the number, shape, and position of STM maxima are strongly dependent on the bias voltage and tunneling current. At biases higher than  $+2 \text{ V}$ , only a single protrusion per  $2 \times 3$  unit is seen in STM images, in agreement with earlier observations in Ref. 20. At lower bias voltages, additional features can be discerned in the images in the empty-state mode. The tunneling current

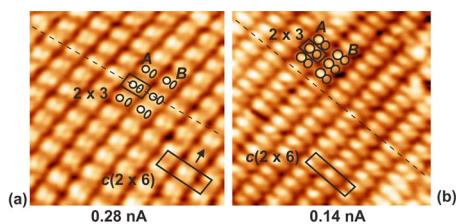


FIG. 3. (Color online) Empty-state ( $V = +1.8$  V) STM images as function of tunneling current. (a)  $I = 0.28$  nA,  $8.4$  nm  $\times$   $8.4$  nm. (b)  $I = 0.14$  nA,  $9.1$  nm  $\times$   $8.9$  nm. There are two nonequivalent protrusions  $A$  and  $B$  in the  $2 \times 3$  unit cell. The mirror-symmetry plane is shown by dot line.

also affects the corrugation of the  $2 \times 3$  structure in the unoccupied orbitals. The most pronounced effect is found at  $+1.8$  V. Two high-resolution STM images taken at this bias voltage are shown in Fig. 3. The image shown in Fig. 3(a) was acquired at a tunneling current of  $0.28$  nA and that shown in Fig. 3(b) was acquired at  $0.14$  nA. At the higher current, the  $2 \times 3$  surface shows up a building block consisting of two nonequivalent maxima with different shapes and brightness. The protrusion  $A$  exhibits almost round shape and slightly higher brightness than the protrusion  $B$  which is elongated in the  $2 \times$  direction. The difference in height of these protrusions is about  $0.1$  Å, and their lateral separation is  $a$ . Note that a local  $c(2 \times 6)$  periodicity can be found on this surface. It arises from a half-period shift of every second row along the direction of  $2 \times$  periodicity, as shown by the arrow in Fig. 3(a). That is, the  $c(2 \times 6)$  structure appears when the neighboring rows of  $2 \times 3$  reconstruction are out of phase. Since both the  $2 \times 3$  and  $c(2 \times 6)$  phases exhibit the same building blocks, these structures are closely related to each other.

At the lower current [Fig. 3(b)], the registry of  $A$  and  $B$  basically remains identical to that of Fig. 3(a). However, the difference in height of these protrusions becomes higher (about  $0.3$  Å) and, in addition, their shape is slightly modified at  $0.14$  nA. The variation of STM images as a function of tunneling current was recently observed also for the Si(100) $2 \times 3$ -Na surface.<sup>8</sup> It was reported that the vertical position of Na atoms is very sensitive to a tip-induced electric field whose variation is associated with the change of tunneling current rather than that of bias voltage. In particular, the “Na subunit” of the  $2 \times 3$  unit cell was found to be noticeably lower in high-current filled-state STM images, whereas the Si atoms are less sensitive to the electric field.<sup>26</sup> In the  $2 \times 3$ -Eu case, it is not possible to conclude which of the two observed protrusions,  $A$  or  $B$ , is more sensitive to the electric field. However, it should be emphasized that the Eu-induced structures observed in both the STM images at  $+1.8$  V in Fig. 3 preserve a mirror-symmetry plane along the direction of  $\times 3$  periodicity, and no mirror-plane symmetry is found in the orthogonal ( $2 \times$ ) direction.

At lower biases, both the appearance and symmetry of empty-state STM images drastically change. Figure 4 shows the images obtained at  $+1.4$  V (a) and  $+1.0$  V (b). It is clearly seen that one of the structural elements of the  $2 \times 3$  unit cell in these images is a bright pillow-shaped protrusion

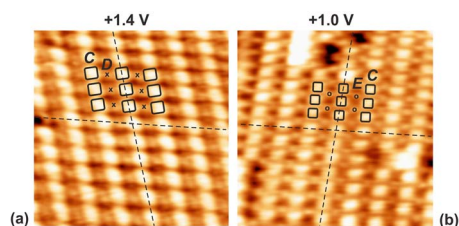


FIG. 4. (Color online) Empty-state STM images of  $2 \times 3$ -Eu at lower biases ( $I = 0.26$  nA). (a)  $V = +1.4$  V. The area is  $6.7$  nm  $\times$   $6.7$  nm. (b)  $V = +1.0$  V. The area is  $7.4$  nm  $\times$   $7.4$  nm. The mirror-symmetry planes are shown by dot lines.

(labeled  $C$ ). The registry of this protrusion is identical to that of  $A$  in Fig. 3. The other structural element is a dim protrusion labeled  $D$  in Fig. 4(a) and  $E$  in Fig. 4(b). The spatial locations of  $D$  and  $E$ , however, differ from each other as well as from that of protrusion  $B$  in Fig. 3. The protrusion  $D$  is situated halfway the neighboring protrusions  $C$  in Fig. 4(a), whereas the protrusion  $E$  is shifted with respect to  $D$  by  $a$  in the  $2 \times$  direction, as shown in Fig. 4(b). The STM images at  $+1.4$  and  $+1.0$  V, in contrast to those at  $+1.8$  V, reveal the mirror-plane symmetry in both the  $\times 3$  and  $2 \times$  directions.

Since the STM images observed at  $+1.8$  V (Fig. 3) and  $+1.0$ / $+1.4$  V (Fig. 4) reveal the nonequivalent symmetries, it can be expected that these images are due to different substructures of the Eu/Si(100)- $2 \times 3$  phase, i.e., they reflect the structural and electronic properties of different elements of this reconstruction. To obtain additional information, we acquired the dual-polarity images from the Eu/Si(100) surface at  $0.1$  ML where the Si substrate is not completely covered with the  $2 \times 3$  phase. At this coverage, the Si dimer rows of the bare Si surface can be detected by STM at both positive and negative polarities. Figures 5(a) and 5(b) depict almost the same areas of  $0.1$ -ML Eu/Si surface at biases of  $-1.8$  and  $+1.0$  V, respectively. In the filled states [Fig. 5(a)], the Eu-induced phase appears as separate protrusions lined up in rows running perpendicular to the direction of bright stripes (marked by arrows) which are the Si dimer rows. The distance between the protrusions is  $2a$ , and we therefore assume that these protrusions are precursors of  $2 \times 3$  phase and can be associated with the presence of Eu atoms. In the empty states [Fig. 5(b)], the Si dimer rows are also seen, however, the dark channels, in which the Eu-associated protrusions were found in the filled states in Fig. 5(a), appear empty. Hence, we suggest that the image at  $+1.0$  V in Fig. 5(b) is mostly contributed by the electronic states localized

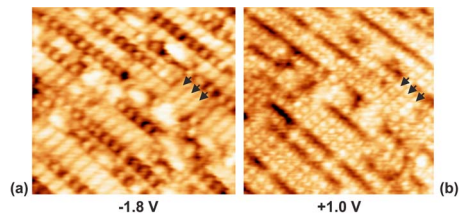


FIG. 5. (Color online) STM images taken from almost the same surface area at  $0.1$  ML Eu in both occupied and unoccupied states. (a)  $V = -1.8$  V,  $I = 0.41$  nA. (b)  $V = +1.0$  V,  $I = 0.46$  nA. The Si dimer rows on the bare Si substrate are marked by arrows.

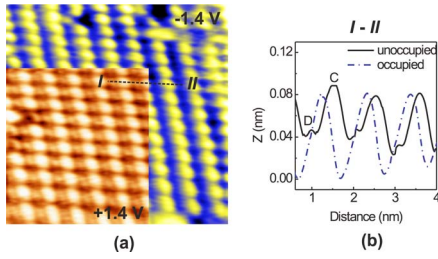


FIG. 6. (Color online) (a) Dual-polarity STM image (9.2 nm  $\times$  9.2 nm) of  $2 \times 3$ -Eu phase at  $V = +1.4$  V/ $-1.4$  V. The structure shown in the left bottom corner is observed in the empty-state mode. (b) Line profiles  $I$ - $II$  taken in both the empty- and filled-state modes. See the text for details.

on the Si atoms. The similar results are found also at a bias voltage of  $+1.4$  V. Thus we expect that the empty-state images of the  $2 \times 3$  surface, taken at  $+1.0$  and  $+1.4$  V (Fig. 4), reflect mostly the Si arrangement of the  $2 \times 3$ -Eu phase. In contrast, the images at  $+1.8$  V (Fig. 3), which indicate the different symmetry and registry of protrusions, are assumed to reflect the adsorption geometry of the Eu overlayer.

Finally, we compare the registry of STM features on the  $2 \times 3$ -Eu surface at positive and negative bias polarities. Figure 6 illustrates the location of protrusions, observed in the empty-state ( $+1.4$  V) and filled-state ( $-1.4$  V) images, with respect to each other. In this figure, a fragment of the empty-state image (the left bottom corner) is superimposed on the filled-state image. (Note that these images were obtained simultaneously in the dual-polarity mode.) As seen, the bright protrusions observed in the empty-state mode are slightly shifted along the  $\times 3$  direction with respect to the protrusions in the filled-state mode. The difference in position of these maxima is clearly seen from comparing two line profiles  $I$ - $II$  measured along equivalent lines in the empty- and filled-state images. Thus the filled-state features are roughly located in the middle between the bright and dim protrusions (C and D, respectively) in the empty states.

## B. STS

Figure 7 represents the tunneling spectrum  $I$ - $V$  (curve *a*) taken from the  $\text{Si}(100)2 \times 3$ -Eu surface over a well-ordered  $2 \times 3$  domain free of defects. This curve indicates a tunneling gap of  $\sim 0.6$  V. Such behavior is well consistent with the absence of emission at the Fermi level in the resonant Eu  $4f$  emission spectrum of this reconstruction (not shown). Thus the  $\text{Si}(100)2 \times 3$ -Eu surface is semiconducting. We also note in passing that the tunneling gap in the  $I$ - $V$  spectrum of Fig. 7 is very similar to that observed for the clean  $\text{Si}(100)2 \times 1$  surface with buckled dimers.<sup>27</sup>

More detailed information about the electronic structure of the  $2 \times 3$ -Eu phase can be extracted from the  $(dI/dV)/(I/V)$  spectrum. It approximately reflects the local density of states (LDOS) of a surface.<sup>28</sup> This similarity, however, is only limited to peak positions, but the intensities of peaks are dependent on the tip-substrate configuration and normalization procedure.<sup>29</sup> To interpret the  $(dI/dV)/(I/V)$  spectrum of the  $2 \times 3$  reconstruction properly, we compare

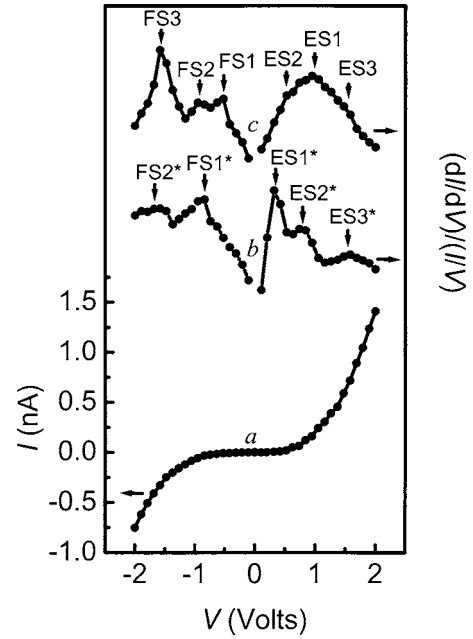


FIG. 7. (a) Tunneling spectrum  $I$ - $V$  of  $2 \times 3$ -Eu surface. (b)  $(dI/dV)/(I/V)$  spectrum of  $2 \times 3$ -Eu. (c)  $(dI/dV)/(I/V)$  spectrum of clean  $\text{Si}(100)2 \times 1$  surface.

it with the analogous spectrum obtained for the clean  $\text{Si}(100)2 \times 1$  surface with the buckled dimers. In Fig. 7, the  $(dI/dV)/(I/V)$  spectra taken from both the Eu-induced  $2 \times 3$  and clean  $2 \times 1$  surfaces (curves *b* and *c*, respectively) are shown. In previous experimental and theoretical studies, three occupied and three unoccupied surface-state bands (i.e.,  $\pi_1$ ,  $\pi_2$ ,  $\pi_1^*$ , and  $\pi_2^*$  dangling-bond states, and  $\sigma$  and  $\sigma^*$  Si-Si backbond states) were identified in the  $(dI/dV)/(I/V)$  spectrum of the clean  $\text{Si}(100)$  surface.<sup>30-34</sup> In the present study, the  $(dI/dV)/(I/V)$  spectrum of  $\text{Si}(100)2 \times 1$  (curve *c* in Fig. 7) reasonably agrees with those in the literature. In the filled states, it displays a sharp peak FS3 at around  $-1.6$  V and two resolved peaks FS1 and FS2 at  $-0.55$  and  $-0.95$  V, which can be straightforwardly assigned to the  $\sigma$  Si-Si bond state and  $\pi_1$  and  $\pi_2$  dangling-bond states, respectively, in good agreement with the calculations in Ref. 34. Note that  $\pi_1$  and  $\pi_2$  dangling-bond features were not resolved in experiment previously. In the empty states, we find a broad peak centered at  $+0.95$  V with weak shoulders at around  $+0.5$  and  $+1.5$  V, i.e., there are the features ES1, ES2, and ES3, respectively. Although the ES1, ES2, and ES3 features are not fully resolved in the clean spectrum, we assign them, based on the previous results in Refs. 30-34, to the  $\pi_2^*$  and  $\pi_1^*$  dangling-bond states and  $\sigma^*$  Si-Si bond state, respectively. For the  $2 \times 3$ -Eu phase, the  $(dI/dV)/(I/V)$  spectrum (curve *b* in Fig. 7) undergoes some remarkable changes. We identify the following states based on this spectrum. (i) In the filled states, two peaks FS1\* and FS2\* are observed at around  $-0.9$  and  $-1.75$  V, respectively and (ii) in the empty states, a strong peak ES1\* is observed at around  $+0.35$  V, and two weak peaks ES2\* and ES3\* are found at around  $+0.8$  and  $+1.5$  V, respectively. Thus, the Eu-induced  $2 \times 3$  reconstruction removes the  $\pi_1^*$  and  $\pi_2^*$  dangling-bond states localized on the buckled-down dimer atom of the clean Si surface

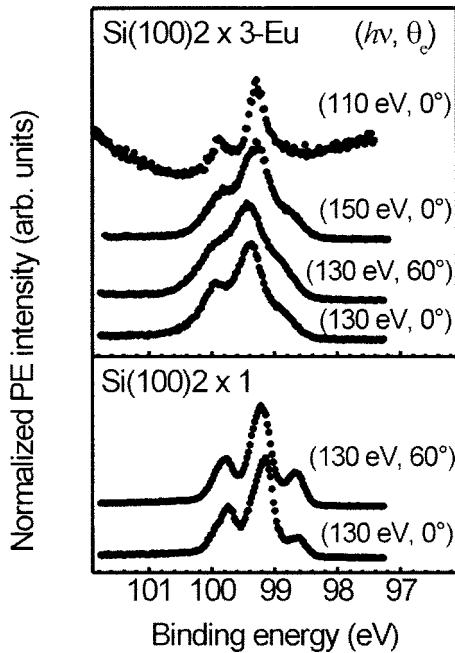


FIG. 8. Normalized Si  $2p$  core-level spectra of clean Si(100) $2 \times 1$  (bottom panel) and Eu-induced Si(100) $2 \times 3$  (top panel) surfaces for various experimental conditions ( $h\nu, \theta_e$ ).

(curve *c*), and induces the unoccupied states at +0.35 and +0.8 V (ES1\* and ES2\* in curve *b*, respectively). Consequently, we assume that the buckled dimers of the clean Si are destroyed upon the formation of the  $2 \times 3$ -Eu phase.

### C. Si $2p$ core level

In order to examine the structural and electronic properties of the  $2 \times 3$ -Eu reconstruction more thoroughly, the Si  $2p$  core-level spectroscopy was also employed. We measured surface core-level shifts (SCLS) in the Si  $2p$  core-level spectra because they can give valuable information on the bonding configurations and charge states of Si atoms in the reconstruction. The Si  $2p$  spectra of the Si(100) $2 \times 3$ -Eu surface were measured at the photon energies  $h\nu=110, 130,$  and  $150$  eV and the emission angles  $\theta_e=0^\circ$  and  $60^\circ$  to vary the surface and bulk sensitivities. In order to justify the procedure of Si  $2p$  spectrum deconvolution as well as the interpretation of fitting results, we also recorded the Si  $2p$  spectra from the clean Si(100) $2 \times 1$  surface at the experimental conditions of  $(h\nu, \theta_e)=(130 \text{ eV}, 0^\circ)$  and  $(130 \text{ eV}, 60^\circ)$ . Figure 9 shows the raw spectra of both surfaces. The incidence angle of photon flux was fixed at  $45^\circ$  to the surface normal, and the spectra were normalized to their maximum intensities. As seen at the bottom of Fig. 9, the clean spectra exhibit a typical Si  $2p$  spin-orbit doublet line shape with the well-resolved shoulder on the lower binding-energy side with respect to the main peak. This shoulder is known to be due to the buckled-up dimer atoms.<sup>35</sup> It is more prominent under the most surface-sensitive condition  $(h\nu, \theta_e)=(130 \text{ eV}, 60^\circ)$ . For the  $2 \times 3$ -Eu reconstruction, the spectral line shape changes significantly, as shown at the top of Fig. 9. The  $2 \times 3$  spectra are seen to be rather structureless, as compared

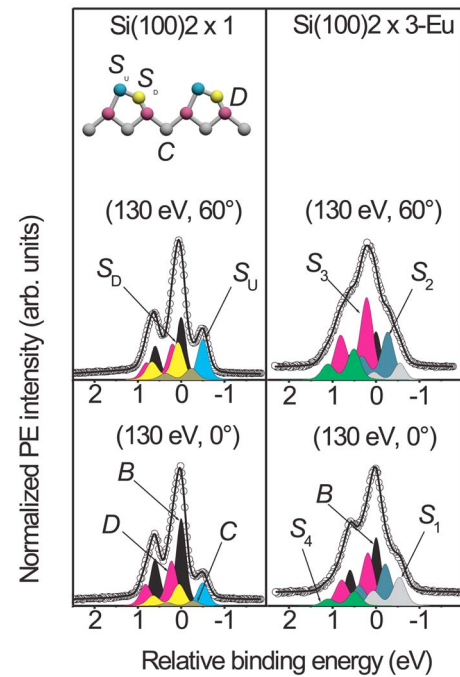


FIG. 9. (Color online) Deconvolution of Si  $2p$  spectra from clean Si(100) $2 \times 1$  and Eu-stabilized  $2 \times 3$  surfaces (left and right panels, respectively) at  $h\nu=130$  eV and normal ( $\theta_e=0^\circ$ ) and grazing emissions ( $\theta_e=60^\circ$ ). Raw data are shown by open circles and fitting curves by solid lines. Shaded doublets represent the Si  $2p$  bulk (*B*) and surface ( $S_u, S_d, D, C, S_1, S_2, S_3,$  and  $S_4$ ) components. The atomic structure of the clean surface (side view) is illustrated on top of the left panel.

to the clean spectra. Especially, the "triangular" line shape of the  $2 \times 3$  spectra is clearly observed at the most surface-sensitive condition  $(h\nu, \theta_e)=(130 \text{ eV}, 60^\circ)$ . A deep valley between Si  $2p_{1/2}$  and  $2p_{3/2}$  peaks, which is clearly seen in the most bulk-sensitive spectrum at  $(h\nu, \theta_e)=(110 \text{ eV}, 0^\circ)$ , disappears with increasing the surface sensitivity. Consequently, we presume the existence of surface-related component(s) shifted to the higher-binding energy with respect to the bulk component. Another surface component(s) shifted to the lower-binding energy can be suggested because of the presence of shoulder on the lower-binding-energy side of the main peak in the  $2 \times 3$  spectra. In addition, we remark that at the most bulk-sensitive condition of  $(h\nu, \theta_e)=(110 \text{ eV}, 0^\circ)$ , the binding energy of the main peak is 0.14 eV higher than that of the most bulk-sensitive  $2 \times 1$  spectrum (not shown). Since both spectra are mostly contributed by the bulk component *B* and the binding energy was referred to the Fermi level in our measurements, this shift means that the Fermi level position in the band gap moves upward by 0.14 eV after the formation of the  $2 \times 3$ -Eu phase.

Since the fitting parameters and core-level shifts in the Si  $2p$  spectra of the clean Si(100) surface are well established,<sup>35</sup> we first decompose the clean spectra, testing the deconvolution procedure applied in this study. The background of the spectra was subtracted by Shirley's method. The fitting functions were spin-orbit-split doublets with the Voigt peaks. Some parameters were determined from the deconvolution of the most bulk-sensitive spectrum at  $(h\nu, \theta_e)=(110 \text{ eV}, 0^\circ)$ . It

was found that the spin-orbit splitting, branching ratio, and Lorentzian width (LW) of the bulk component  $B$  are 0.602 eV, 0.50, and 0.085 eV, respectively. These parameters were then fixed for all the components. The Gaussian width (GW) of  $B$  was determined to be 0.225 eV, and it was allowed to slightly increase for the surface components, since besides the instrumental resolution, the GW is controlled by other parameters such as the phonon broadening and surface inhomogeneity that are slightly enhanced for the surface atoms, as compared to the bulk ones.<sup>36</sup> In addition, some physically reasonable constraints were applied to reduce the ambiguity of our fitting procedure. The intensity ratio of components  $S_u$  and  $S_d$ , whose atomic origins are the buckled-up and buckled-down dimer atoms, was 1:1. The intensity of component  $D$ , whose atomic origin is the second-layer atom, was kept not larger than the total intensity of  $S_u$  and  $S_d$ . Finally, the GW of  $S_u$ , which can be evaluated from the surface-sensitive spectrum at the grazing emission, was suggested to be the upper limit for the surface components. The number and shifts of surface components were variable parameters. All the fitting parameters, except the intensities of components, were fixed between the various emission angles and photon energies of the individual surface. Applying such a self-consistent approach, we found the best reproducibility of clean spectra using one bulk ( $B$ ) and four surface components  $S_u$  (SCLS of  $-0.49$  eV),  $S_d$  (0.06 eV),  $D$  (0.21 eV), and  $C$  ( $-0.26$  eV), as shown in the left panel of Fig. 9 for two experimental conditions  $(h\nu, \theta_e) = (130 \text{ eV}, 0^\circ)$  and  $(130 \text{ eV}, 60^\circ)$ . The GW's of surface components were found between 0.250 and 0.265 eV. The fitting results of the clean surface are in good agreement with Ref. 35. Besides these five components, two very weak Gaussian-like loss features shifted by +1.3 and +1.9 eV to the higher-binding energy with respect to  $B$  were also introduced to slightly improve the fit of the higher-binding-energy tail of spectra (not shown). The origin of these minor features was discussed earlier.<sup>37,38</sup> Since their introducing did not affect on the other fitting parameters practically, we do not consider the loss features hereafter.

Based on the fitting results for the clean surface, the deconvolution of  $2 \times 3$  spectra was started with introducing three surface components with unfixed SCLS, in addition to the bulk component  $B$ . The spin-orbit splitting, branching ratio, and LW were the same as for the clean spectra, and they were confirmed by reproducing the spectral line shape under the most bulk-sensitive condition with the dominating component  $B$ . The GW of  $B$  was constant through all the clean and  $2 \times 3$  spectra, whereas for the surface components, the GW was let to slightly increase in the  $2 \times 3$  spectra. The line shape of surface-sensitive  $2 \times 3$  spectra was not satisfactorily fitted using three surface components, in addition to  $B$ . Adding a fourth surface component enabled us to obtain a good reproducibility of the spectra, and further introducing of additional components did not improve the quality of results significantly. Among these four components, one component ( $S3$ ) has a positive SCLS of 0.21 eV, which is equal to that of components  $D$  found for the clean Si. For this reason, we assume that  $S3$  and  $D$  have a common origin, i.e., they both are due to the second-layer Si atoms. The other components are  $S1$ ,  $S2$ , and  $S4$  with SCLS's of  $-0.54$ ,

$-0.24$ , and 0.51 eV, respectively. The GW's of these components are between 0.250 and 0.275 eV. The SCLS of  $S1$  is close to that of  $S_u$  ( $-0.49$  eV) originating from the buckled-up dimer atom on the clean sample. However, the  $2 \times 3$  spectra reveal no component with the SCLS of around 0.06 eV, which can correspond to the buckled-down dimer atom. Therefore, it can be concluded that the asymmetric Si dimers found on the Si(100) surface are removed in the  $2 \times 3$ -Eu reconstruction, and the atomic origin of  $S1$  is different from that of  $S_u$ . Also, we find that the atomic origin of  $S2$  ( $-0.24$  eV) is different from that of  $C$  ( $-0.26$  eV) for clean Si, because  $C$  stems from half the third-layer atoms of the clean Si substrate,<sup>35</sup> and the intensity of  $S2$  in the  $2 \times 3$  spectra is higher by several times than the intensity of  $C$  in the clean spectra. Finally, the component  $S4$  has the SCLS of 0.51 eV, and therefore, the atomic origin of this component is different from those of the clean surface. Since the core-level shifts of  $D$  and  $S3$  are identical, we suggest that the second layer of Si substrate is not affected by Eu adsorption in the  $2 \times 3$ -Eu system. Therefore, the Eu atoms are directly bonded to the first-layer Si atoms in this reconstruction, and the  $S1$ ,  $S2$ , and  $S4$  components can be assigned to these Si atoms, agreeing with earlier core-level studies of the Si(001) $2 \times 3$ -In (Ref. 39) and  $-Mg$  (Ref. 14) systems, where it was found that the electronic and geometric properties of the second Si layer are not altered significantly upon In and Mg adsorption. In these systems, the similar components  $D$  with SCLS's of 0.19 eV for In (Ref. 39) and 0.25 eV for Mg (Ref. 14) were identified. However, the total number of Si  $2p$  surface components for  $2 \times 3$ -In and  $-Mg$  is different from that of  $2 \times 3$ -Eu in the present study, and we presume that the atomic geometry of  $2 \times 3$ -Eu is nonequivalent to those of  $2 \times 3$ -In and  $2 \times 3$ -Mg.

#### IV. DISCUSSION

In this section, we first discuss the results shown in Sec. III in the context of some structural models reported earlier for other metal-induced Si(100) $2 \times 3$  reconstructions, and then propose an atomic model of Si(100) $2 \times 3$ -Eu. As remarked in Sec. I, the models proposed for the  $2 \times 3$ -Na and  $-Ba$  surfaces in Refs. 8 and 16 suggest that the Si arrangements of these reconstructions are similar to that of the H-terminated Si(100) $1 \times 3$  surface<sup>25</sup> [Fig. 10(a)]. Both the models of  $2 \times 3$ -Na and  $2 \times 3$ -Ba, as shown in Figs. 10(b) and 10(c), reveal the mirror-symmetry plane in the  $\times 3$  direction and no mirror-symmetry plane in the orthogonal  $2 \times$  one, which makes them consistent with the empty-state STM images of  $2 \times 3$ -Eu at +1.8 V. In the model of  $2 \times 3$ -Na (Ref. 8), alternate Si-dimer and Si-atom rows arrange the  $\times 3$  periodicity in the  $[011]$  direction. The additional structural element of  $2 \times 3$ -Na unit cell is an extra Si dimer on the top of the  $1 \times 3$  backbone. Thus the atomic model in Fig. 10(b) suggests five nonequivalent Si surface atoms (one atom in the topmost layer, three atoms in the second layer, and one atom in the third layer), and therefore, five surface components are expected to appear in Si  $2p$  core-level spectra from such a structure. In this study, the number of Si  $2p$  surface components for the  $2 \times 3$ -Eu surface, as shown in Sec. III, is

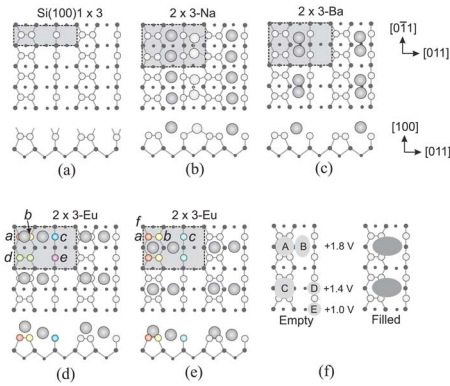


FIG. 10. (Color online) Atomic structure models of (a) H-terminated Si(100) $1 \times 3$  surface (from Ref. 25), (b) Si(100) $2 \times 3$ -Na reconstruction (from Ref. 8), (c) Si(100) $2 \times 3$ -Ba reconstruction (from Ref. 16), and (d),(e) Si(100) $2 \times 3$ -Eu reconstruction. Metal atoms are shown by large circles. Eu atoms are adsorbed at the bridge/cave sites in the model (d) and the pedestal/valley bridge sites in the model (e). (f) Schematic diagram showing the registry of STM protrusions for the  $2 \times 3$ -Eu surface.

different. Moreover, the filled-state STM images of  $2 \times 3$ -Eu are found to be rather different from those of  $2 \times 3$ -Na in Ref. 8. Therefore, we suppose that the atomic structure of the  $2 \times 3$ -Eu phase cannot be described in terms of the model in Fig. 10(b).

In the model of the  $2 \times 3$ -Ba surface, the Ba atoms sit in the channels between dimeric-Si and mono-Si rows, as shown in Fig. 10(c). The  $2 \times$  periodicity of this reconstruction originates from the dimerization of Ba atoms along the  $[0-11]$  direction. In such a configuration, there are three nonequivalent first-layer Si atoms, which agrees with the present Si  $2p$  core-level results indicating three first-layer components  $S1$ ,  $S2$ , and  $S4$ . However, the filled-state STM images of the  $2 \times 3$ -Eu phase are very different from those of the  $2 \times 3$ -Ba system in Ref. 16 (e.g., the latter show a pair of elliptical protrusions and a pair of round ones per  $2 \times 3$  unit cell, in contrast to one oval-shaped protrusion in this study), thus suggesting the difference in atomic arrangement of these reconstructions. Moreover, we notice that in the model of Fig. 10(c), the average distance between neighboring Ba atoms along a  $2 \times$  row is  $a$ , and the  $2 \times$  periodicity results from the dimerization of these atoms. As for the  $2 \times 3$ -Eu case, such atomic rows, in our opinion, would appear in empty-state STM images as unresolved stripes, as it was recently found for the similar “ $2$ ” rows in the  $5 \times “2”$ ,  $7 \times “2”$ , and  $9 \times “2”$  structures on the Eu/Si(111) surface.<sup>40</sup> In this study, however, the  $2 \times$  rows in the empty-state images indicate a clear modulation in brightness with well-resolved maxima (Figs. 3 and 4). Thus, the model of Fig. 10(c) cannot be adopted for the Si(100) $2 \times 3$ -Eu surface. In addition, the other atomic models proposed for the  $2 \times 3$ -Mg,<sup>14</sup> -Sr,<sup>12</sup> and -In (Ref. 39 and references therein) phases on Si(100) (not shown) also disagree with the present data because the symmetry of these structures is different from that observed for  $2 \times 3$ -Eu in the empty-state STM images at +1.8 V (Fig. 3) as well as the number of surface components in Si  $2p$  core-level spectra from the Mg- and

In-induced  $2 \times 3$  reconstructions is different from that of  $2 \times 3$ -Eu.

In Figs. 10(d) and 10(e), we consider two plausible structural models for the Eu/Si(100) $2 \times 3$  phase, both of which are based on the model of the Si(100)- $1 \times 3$  surface in Fig. 10(a). As the most stable sites for metal atoms on the intact Si(100) $2 \times 1$  surface are the cave and valley bridge sites (Refs. 14 and 26, and references therein), we speculate that these sites are favorable for Eu atoms in the  $1 \times 3$  Si backbone. However, only half of such sites can be occupied because the mirror-plane symmetry along the  $\times 3$  direction is broken in the  $1/3$ -ML  $2 \times 3$ -Eu reconstruction, as found in the STM images at +1.8 V in Fig. 3. It means that  $1/6$  ML of Eu atoms (i.e., half the Eu atoms) can sit at the cave/valley bridge sites, and the other half of Eu atoms reside at the bridge/pedestal sites, as shown in Figs. 10(d) and 10(e), respectively. Both these atomic geometries suggest two different sites for the Eu atoms, in agreement with the STM results in Fig. 3. Note that in both models, the Eu atoms are not bonded to the second-layer Si atoms (i.e., the  $f$  atoms) directly, and thus the component  $D$  ( $S3$ ) in the Si  $2p$  spectra, as remarked before, is unchanged upon Eu adsorption. To discriminate between these two models, we count the number of nonequivalent Si surface atoms with different bonding environments in both structures. The model in Fig. 10(d) shows five first-layer Si atoms ( $a$ ,  $b$ ,  $c$ ,  $d$ , and  $e$ ), and the model in Fig. 10(e) does three first-layer Si atoms ( $a$ ,  $b$ , and  $c$ ). Therefore, based on the correlation between the number of Si  $2p$  surface components and the number of nonequivalent Si surface atoms, only the model in Fig. 10(e) can explain the present Si  $2p$  core-level results reasonably. In this model, the  $a$ ,  $b$ , and  $c$  atoms, which have different bonding sites, are suggested to cause the  $S1$ ,  $S2$ , and  $S4$  components with three different SCLS's ( $-0.54$ ,  $-0.24$ , and  $+0.51$  eV, respectively). As the  $b$  atom is directly bonded to two Eu atoms, and the  $a$  and  $c$  atoms are each bonded to one Eu atom, it can be expected that a larger charge transfer occurs from Eu to the  $b$  atom than to the  $a$  and  $c$  atoms. Hence, within the initial-state effects, the component  $S1$  with the lowest-binding energy can be assigned to the  $b$  atoms and the two other first-layer components with the higher-binding energies to the  $a$  and  $c$  atoms. For more detailed interpretation of the atomic origin of  $S2$  and  $S4$  and solving physical phenomena behind their core-level shifts, SCLS calculations using the initial- and final-state theories are needed.

Finally, we discuss the STM and STS results in the context of the model in Fig. 10(e). In this model, the geometry of Eu overlayer has only one mirror-symmetry plane which is along the  $\times 3$  direction. Obviously, this is in agreement with the symmetry of the empty-state images at +1.8 V (Fig. 3). The registry of two protrusions,  $A$  and  $B$ , in these images [see Fig. 10(f)] is consistent with the positions of Eu atoms in Fig. 10(e). Thus the model of Fig. 10(e) reasonably accounts for the STM images at +1.8 V, supporting the proposition in Sec. III A that they reflect the adsorption geometry of Eu atoms.

When the bias voltage is decreased, the empty-state STM images at +1.4 and +1.0 V (Fig. 4) reveal two mirror-symmetry planes in the  $2 \times$  and  $\times 3$  directions and are expected to be due to the Si arrangement of the  $2 \times 3$ -Eu struc-

ture, as assumed in Sec. III A. This is also in agreement with the model in Fig. 10(e). The registry of protrusions *C*, *D*, and *E* found in the STM images of Fig. 4 is shown in Fig. 10(f), and we speculate that these images reflect the geometric and electronic properties of the first Si layer interacting with Eu in the  $2 \times 3$  reconstruction. Interestingly, the  $ES2^*$  and  $ES3^*$  unoccupied states were found in the  $(dI/dV)/(I/V)$  spectrum from the  $2 \times 3$  surface at +0.8 and +1.5 V. Tentatively, it is believed that the former state contributes mostly to the STM image at +1.0 V and the latter to the image at +1.4 V. Because the protrusion *D* observed in the image at +1.4 V and the protrusion *E* observed in the image at +1.0 V are laterally separated, it is obvious that the spatial distributions of  $ES2^*$  and  $ES3^*$  states are nonidentical. The third empty state  $ES1^*$  is found at +0.35 V where the tunneling current is negligibly small. For this reason, the nature of this state is unclear and will not be discussed in this investigation. In the filled states, the STM images are not found to be bias dependent. Therefore, the spatial distributions of  $FS1^*$  and  $FS2^*$  states identified in the  $(dI/dV)/(I/V)$  spectrum at  $-0.9$  and  $-1.75$  V seem to be similar. The registry of oval-shaped protrusions observed in the filled-state images is shown in Fig. 10(f). Thus the model of Fig. 10(e) reasonably accounts for the main experimental features obtained in this study. Obviously, it is different from the models proposed earlier for the other metal-induced  $Si(100)2 \times 3$  phases, and therefore, the adsorbate atoms may play a crucial role in the formation process of  $M/Si(100)2 \times 3$  reconstruction. It is likely that the electronic and magnetic properties of Eu should be taken into account to understand the role of this metal in forming the  $Eu/Si(100)2 \times 3$  reconstruction.

## V. CONCLUSION

In conclusion, we have investigated the atomic and electronic structure of the Eu-induced  $Si(100)2 \times 3$  surface phase by STM, STS, and Si  $2p$  core-level photoelectron spectroscopy using synchrotron radiation. It is shown that the STM images of this reconstruction drastically depend on the bias

voltage and tunneling current. In the filled-state mode, a single elliptical protrusion per  $2 \times 3$  unit cell is found. In the empty-state mode, the appearance of the  $2 \times 3$  unit is strongly affected by the bias voltage and tunneling current. The empty-state protrusions *A* and *B* at +1.8 V are associated with two nonequivalent Eu atoms in the  $2 \times 3$  unit. The structure seen at this bias voltage has one mirror-symmetry plane along the  $2 \times$  direction. At +1.4 V (+1.0 V), the STM images include the protrusions *C* and *D* (*C* and *E*) and are proposed to reflect the arrangement of the Si subsystem of the  $2 \times 3$ -Eu reconstruction. These images, in contrast to those at +1.8 V, reveal two mirror-symmetry planes along both the  $2 \times$  and  $\times 3$  directions. The STS results show that the  $Si(100)2 \times 3$ -Eu surface is semiconducting. Based on the normalized conductance spectra  $(dI/dV)/(I/V)$ , we have identified two occupied states  $FS1^*$  and  $FS2^*$  at  $-0.9$  and  $-1.75$  V, and three unoccupied states  $ES1^*$ ,  $ES2^*$ , and  $ES3^*$  at +0.35, +0.8, and +1.5 V, respectively. The Si  $2p$  core-level spectra taken at various photon energies and emission angles are fitted by the bulk component *B* and four surface components *S1*–*S4* with SCLS's of  $-0.54$ ,  $-0.24$ ,  $+0.21$ , and  $+0.51$  eV. The *S1*, *S2*, and *S4* components are found to originate from the topmost-layer Si atoms, whereas *S3* arises from the second-layer Si atoms. It is shown that the core-level shift of *S3* is identical to that of analogous component *D* observed for the clean  $Si(100)2 \times 1$  surface, and therefore, the second layer of Si substrate is not assumed to be altered upon Eu adsorption. Based on these results and data available in the literature, a structural model for the  $2 \times 3$ -Eu surface is proposed and discussed in detail.

## ACKNOWLEDGMENTS

We gratefully acknowledge the experimental support of Dr. T. Balasubramanian and the MAX-lab staff. We thank H. Ollila for the technical assistance. The financial support by the Graduate School of Material Research (GSMR) and the Transnational Access to the Research Infrastructure Program (TARI) are acknowledged. This work has been supported in part by the Academy of Finland (Grant No. 205766).

\*Electronic address: m.kuzmin@mail.ioffe.ru

<sup>1</sup>X. F. Lin, K. J. Wan, and J. Nogami, Phys. Rev. B **47**, 10947 (1993); **47**, 13491 (1993); **49**, 7385 (1994).

<sup>2</sup>H. W. Yeom, I. Matsuda, K. Tono, and T. Ohta, Phys. Rev. B **57**, 3949 (1998).

<sup>3</sup>A. Brodde, Th. Bertrams, and H. Neddermeyer, Phys. Rev. B **47**, 4508 (1993).

<sup>4</sup>G. S. Glander and M. B. Webb, Surf. Sci. **222**, 64 (1989); **224**, 60 (1989).

<sup>5</sup>R. Holtom and P. M. Gundry, Surf. Sci. **63**, 263 (1977).

<sup>6</sup>T. Abukawa, T. Okane, and S. Kono, Surf. Sci. **256**, 370 (1991).

<sup>7</sup>T. Abukawa and S. Kono, Surf. Sci. **214**, 141 (1989).

<sup>8</sup>A. A. Saranin, A. V. Zotov, S. V. Ryzhkov, D. A. Tsukanov, V. G. Lifshits, J.-T. Ryu, O. Kubo, H. Tani, T. Harada, M. Katayama, and K. Oura, Phys. Rev. B **58**, 4972 (1998).

<sup>9</sup>W. C. Fan and A. Ignatiev, Surf. Sci. **253**, 297 (1991).

<sup>10</sup>W. C. Fan, N. J. Wu, and A. Ignatiev, Phys. Rev. B **42**, 1254 (1990).

<sup>11</sup>T. Urano, K. Tamiya, K. Ojima, S. Hongo, and T. Kanaji, Surf. Sci. **357/358**, 459 (1996).

<sup>12</sup>R. Z. Bakhtizin, J. Kishimoto, T. Hashizume, and T. Sakurai, Appl. Surf. Sci. **94/95**, 478 (1996); J. Vac. Sci. Technol. B **14**, 1000 (1996).

<sup>13</sup>Y. Kawashima, H. Takabe, T. Ikeda, H. Itoh, and T. Ichinokawa, Surf. Sci. **319**, 165 (1994).

<sup>14</sup>E. S. Cho, C. H. Lee, C. C. Hwang, J. C. Moon, J. H. Oh, K. Ono, M. Oshima, K. S. An, and C. Y. Park, Surf. Sci. **523**, 30 (2003).

<sup>15</sup>X. Hu, X. Yao, C. A. Peterson, D. Sarid, Z. Yu, J. Wang, D. S. Marshall, R. Droopad, J. A. Hallmark, and W. J. Ooms, Surf. Sci. **445**, 256 (2000).

- <sup>16</sup>K. Ojima, M. Yoshimura, and K. Ueda, *Surf. Sci.* **491**, 169 (2001).
- <sup>17</sup>J. Onsgaard, M. Christiansen, F. Ørskov, and P. J. Godowski, *Surf. Sci.* **247**, 208 (1991).
- <sup>18</sup>M. V. Katkov and J. Nogami, *Surf. Sci.* **524**, 129 (2003).
- <sup>19</sup>M. Kuzmin, R. E. Perälä, P. Laukkanen, R.-L. Vaara, M. A. Mitsu, I. J. Väyrynen, *Appl. Surf. Sci.* **214**, 196 (2003).
- <sup>20</sup>M. Kuzmin, P. Laukkanen, R. E. Perälä, R.-L. Vaara, and I. J. Väyrynen, *Surf. Sci.* **584**, 1 (2005).
- <sup>21</sup>H. W. Yeom, T. Abukawa, M. Nakamura, X. Chen, S. Suzuki, S. Sato, K. Sakamoto, T. Sakamoto, and S. Kono, *Surf. Sci.* **340**, L983 (1995).
- <sup>22</sup>T. Ide, T. Nishimori, and T. Ichinokawa, *Surf. Sci.* **209**, 335 (1989).
- <sup>23</sup>B. Bourguignon, K. L. Carleton, and S. R. Leone, *Surf. Sci.* **204**, 455 (1988).
- <sup>24</sup>A. A. Saranin, A. V. Zotov, V. G. Kotlyar, I. A. Kuyanov, T. V. Kasyanova, A. Nishida, M. Kishida, Y. Murata, H. Okado, M. Katayama, and K. Oura, *Phys. Rev. B* **71**, 035312 (2005).
- <sup>25</sup>Y. J. Chabal and K. Raghavachari, *Phys. Rev. Lett.* **54**, 1055 (1985).
- <sup>26</sup>A. Pomyalov and Y. Manassen, *Surf. Sci.* **382**, 275 (1997).
- <sup>27</sup>A. W. Munz, Ch. Ziegler, and W. Gopel, *Phys. Rev. Lett.* **74**, 2244 (1995).
- <sup>28</sup>J. Tersoff and D. R. Hamann, *Phys. Rev. Lett.* **50**, 1998 (1983); *Phys. Rev. B* **31**, 805 (1985).
- <sup>29</sup>Z.-C. Dong, D. Fujita, and H. Nejoh, *Phys. Rev. B* **63**, 115402 (2001).
- <sup>30</sup>R. J. Hamers, Ph. Avouris, and F. Bozso, *Phys. Rev. Lett.* **59**, 2071 (1987).
- <sup>31</sup>J. J. Boland, *Phys. Rev. B* **44**, R1383 (1991).
- <sup>32</sup>T. Yokoyama and K. Takayanagi, *Phys. Rev. B* **59**, 12232 (1999).
- <sup>33</sup>H. Kageshima and M. Tsukada, *Phys. Rev. B* **46**, 6928 (1992).
- <sup>34</sup>H. Okada, Y. Fujimoto, K. Endo, K. Hirose, and Y. Mori, *Phys. Rev. B* **63**, 195324 (2001).
- <sup>35</sup>E. Landemark, C. J. Karlsson, Y.-C. Chao, and R. I. G. Uhrberg, *Phys. Rev. Lett.* **69**, 1588 (1992).
- <sup>36</sup>M. Borg, M. Birgersson, M. Smedh, A. Mikkelsen, D. L. Adams, R. Nyholm, C.-O. Almbladh, and J. N. Andersen, *Phys. Rev. B* **69**, 235418 (2004).
- <sup>37</sup>C.-P. Cheng, I.-H. Hong, and T.-W. Pi, *Phys. Rev. B* **58**, 4066 (1998).
- <sup>38</sup>H. Koh, J. W. Kim, W. H. Choi, and H. W. Yeom, *Phys. Rev. B* **67**, 073306 (2003).
- <sup>39</sup>H. W. Yeom, T. Abukawa, Y. Takakuwa, Y. Mori, T. Shimatani, A. Kakizaki, and S. Kono, *Phys. Rev. B* **54**, 4456 (1996).
- <sup>40</sup>M. Kuzmin, R.-L. Vaara, P. Laukkanen, R. E. Perälä, and I. J. Väyrynen, *Surf. Sci.* **549**, 183 (2004); M. Kuzmin, P. Laukkanen, R. E. Perälä, R.-L. Vaara, and I. J. Väyrynen, *Phys. Rev. B* **71**, 155334 (2005).